

Temporal Evolution of Flow in Pore-Networks: From Homogenization to Instability

Ahmad Zareei,* Deng Pan,* and Ariel Amir†

School of Engineering and Applied Sciences, Harvard University, Cambridge, MA, 02148

(Dated: June 24, 2021)

We study the dynamics of flow-networks in porous media using a pore-network model. First, we consider a class of erosion dynamics assuming a constitutive law depending on flow rate, local velocities, or shear stress at the walls. We show that depending on the erosion law, the flow may become uniform and homogenized or become unstable and develop channels. By defining an order parameter capturing these different behaviors we show that a phase transition occurs depending on the erosion dynamics. Using a simple model, we identify quantitative criteria to distinguish these regimes and correctly predict the fate of the network, and discuss the experimental relevance of our result.

Fluid flow through a porous medium undergoing a dynamical change in its network of micro-structure is ubiquitous in nature [1–4] as well as in numerous environmental [5–7] and industrial applications [8–11]. The disordered pore structure of a porous medium results in heterogeneously distributed fluid flow between the pores. The boundaries of the pore structure can change dynamically either through erosion or deposition/sedimentation of material. Such heterogeneous changes of the solid structure affect the pore-level fluid flow which in turn affects the dynamical changes to the pore structure. This feedback mechanism along with the initial heterogeneous fluid flow makes it difficult to understand and predict the porous media behavior. Nonetheless, an understanding of the dynamical change is essential to improve any of the porous media applications where the pore network changes over time, including groundwater remediation and precipitation of minerals in rocks [12], biofilm growth in water filtration, and protective filters [13–17], as well as enhanced oil recovery with polymer flooding [18, 19], or water-driven erosion [20, 21].

Network approach— We approach this long-standing problem using a network model for the porous structure[23–29]. The network of pores inside the solid structure is connected together through pore-throats that effectively show resistance to the fluid flow between the pores (Fig. 1a). Network-based models have been shown to successfully capture key properties of fluid flow in a porous material such as the probability distribution of fluid flux [29], the permeability scaling during clogging [30], or the first fluidized path in a porous structure [31]. We consider low-Reynolds fluid flow through the porous network. The fluid flow rate at the edge connecting pores i and j is given by $q_{ij} = C_{ij}(p_i - p_j)$ where p_i, p_j represent pressures at neighboring nodes. Poiseuille’s law implies that the conductance $C_{ij} = \pi r_{ij}^4 / 8\mu l_{ij}$, with r_{ij} and l_{ij} the edge’s radius and length. Initially, we consider a topologically random network of nodes constructed using uniformly distributed nodes in a planar domain connected using Delaunay triangulation (Fig. 1b). The pore-throats or radii of the edges are con-

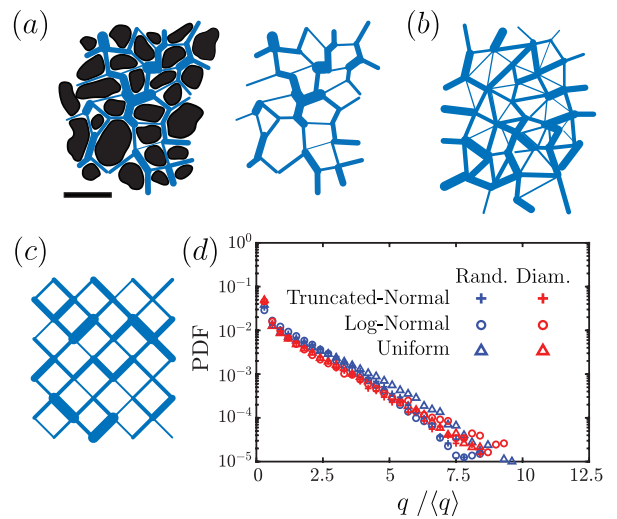


FIG. 1. (a) Cross section of a porous sandstone sample obtained using computerized tomography [22]. The scale in the bottom left shows 1mm. The network of pores and throats is highlighted in blue. In the network model, the pores are represented with nodes and the throats between pores are approximated with tubes. (b) Schematic of a topologically random network. The edge diameters representing the pore-throats are randomly distributed. (c) A structured diamond grid network with a random distribution of edge diameters. (d) The universal probability density function (PDF) of fluid flux for a topologically random (blue) or diamond-grid (red) network of nodes (red) with a random distribution of edge diameter sampled from a uniform (triangles), log-normal (circles), or truncated normal (plus) distribution.

sidered as independent and identically distributed random variables and fluid flow in the edges are obtained by solving for conservation of mass at all nodes given a pressure difference between the nodes on the boundaries (supplementary material S1). Independent of edge radius distribution, the probability density function (PDF) of normalized fluid flux is well described by a single exponential distribution shown in Fig. 1d. The exponential distribu-

tion of fluid flux is similar to earlier experimental and numerical measurements [29, 30, 32] and is a universal feature in random porous networks. Considering a structured diamond-grid of pores (Fig. 1c) which significantly simplifies the geometrical complexity of the network and allows for analytical derivation, one finds that the PDF of normalized fluid flux remains unchanged for various distributions suggesting robustness to network topology (Fig. 1d and supplementary materials S2). In the following, we will study, analytically and numerically, how this universal distribution evolves as the network is modified based on a local constitutive law.

Network evolution— The degradation of the solid skeleton (i.e., erosion) or deposition of material on the pore throats (i.e., clogging) in the network of pores is modeled by the change (increase or decrease) in the radii of the edges connecting the pores which translates into changes in the flow resistance between the pores. The rate of change of the radii depends on local fluid flow parameters, however, the exact dependence is unknown. Different models have been used where erosion is assumed to be locally proportional to shear stress at the walls [33–36], power dissipation by flow [37–39], or local pressure difference [21, 40]. We use a general constitutive model which may implement a diverse set of erosion or clogging dynamics and thus allows us to study the effect of different laws in a unified way.

In order to model erosion in porous media, we consider the abrasion in the throats leading to decrease in the tube radii. We model the dynamics as

$$\frac{dr_{ij}}{dt} = \alpha \frac{|q_{ij}|^m}{r_{ij}^n}, \quad (1)$$

where m, n, α are constants. Different values of m and n along with a positive $\alpha > 0$ correspond to different erosion physics (analogously, $\alpha < 0$ corresponds to clogging). Particularly, the erosion when $m = 1$ and (i) $n = 0$ depends on the amount of flux q_{ij} passing through the edge; (ii) $n = 2$ depends on the local velocities; (iii) $n = 3$ depends on the shear force at the boundary of the throat. Additionally, $m = 2$ and $n = 6$ corresponds to models considered in biological transport networks where the radii changes are proportional to the square of shear stress at the boundary walls [41, 42]. We consider a randomly initialized network with disordered diameters obtained from a uniform distribution (supplementary material S1). The flow inside the pores, PDF of flux in the tubes, and PDF of tube radii are shown in Fig. 2. We assume a constant pressure difference between the left and the right boundaries. In each time step, we increase the local radii of the tubes based on the erosion law introduced in Eq. (1), assuming erosion is linear in the flux ($m = 1$). Later we will consider the network behavior for other powers of m . We continue the simulations until $\langle r \rangle = 2r_0$. The results of the simulations for different

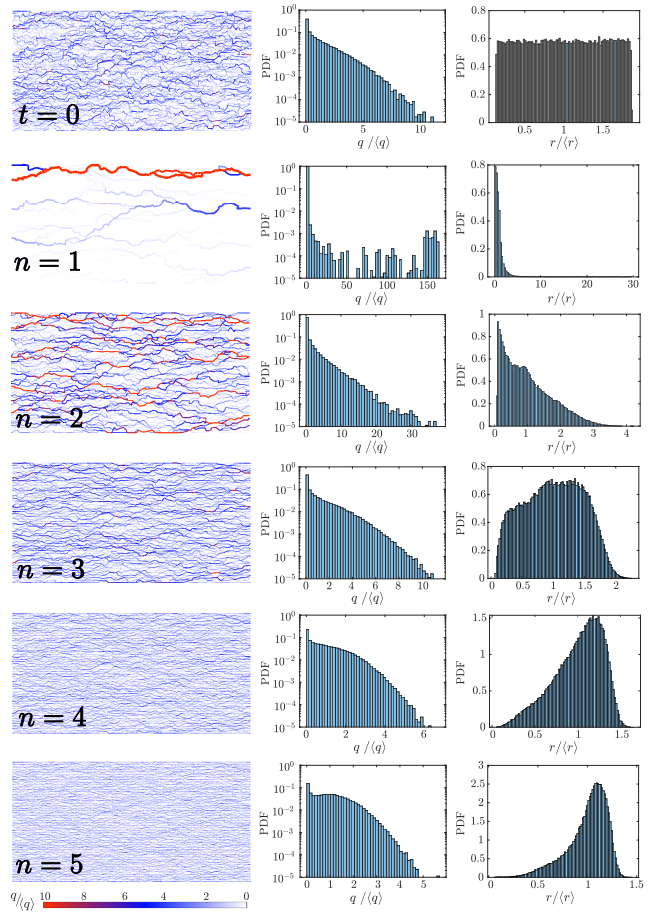


FIG. 2. Erosion in a network of pipes. The initial condition is shown with the label $t = 0$ in the first row. Each row afterward corresponds to the simulation result at $t = T$ where $\langle r_{t=T} \rangle = 2r_0$ with $r_0 = \langle r_{t=0} \rangle$. The erosion law is based on Eq. (1) where $m = 1$ and different powers of n correspond to different models of erosion. The first, second, and third columns are snapshots of the pore network, the PDF of normalized fluid flux $q/\langle q \rangle$, and the PDF of normalized radius $r/\langle r \rangle$ at $t = T$, respectively.

values of n are shown in Fig. 2. When $n = 1$ or 2 , the network develops channels. In such cases, the flow is dominated by a few edges carrying most of the flow while the rest of the network carries almost no flow. This is also reflected by a bimodal radii distribution. In contrast, when $n = 3$ (corresponding to erosion linear in shear), we find that despite the increase in tube radii and absolute flow rates, the normalized flow distribution is hardly affected, maintaining its original exponential form. Increasing n to larger values, $n = 4$ or 5 , we find that the flow pattern in the network moves towards homogenization. Here, the tail of the normalized fluid flux distribution retracts and the coefficient of variation reduces. Similarly, the PDF of the tube diameters becomes narrower.

We found that similar results uphold in a 3d random tube network as well as a 2d topologically ordered (di-

amond grid) network, illustrating the robustness of the results to the network topology (Figs. S2 and S3). Similarly, we found that the results hold also when using an initial narrow distribution of diameters (Fig. S4), showing robustness with respect to the strength of the disorder.

Phase transition and order parameter— To quantify the transition of the network between the channeling instability and homogenization, we define an order parameter

$$\mathcal{O} = \frac{1}{N-1} \left(N - \frac{\left(\sum_{ij} q_{ij}^2 \right)^2}{\sum_{ij} q_{ij}^4} \right), \quad (2)$$

where N is the number of edges. The order parameter defined here is inspired by the participation ratio (PR) employed to quantify the localization of an eigenstate in the analysis of Anderson localization[43]. The order parameter $\mathcal{O} = 0$ when the flux through every edge is identical. On the other hand, when fluid flux becomes highly localized with only a few edges with non-zero flux, $\mathcal{O} \rightarrow 1$. We numerically calculated the order parameter \mathcal{O} for randomly initialized networks, averaged over 20 different realization. The results are shown in Fig. 3a for different amounts of erosion measured by the increase in the average diameter $\langle r \rangle / r_0$. As shown in Fig. 3c, at $n \approx 3$ the order parameter remains unchanged; however for $n > 3$ the order parameter moves toward zero, where the flow becomes more uniform, and for $n < 3$ the order parameter goes toward unity, where channels are developed. This indicates a phase transition at $n = 3$ in the long-time behavior of the network.

Simplified Model— To understand the transition in network behavior during erosion for different powers of n , we focus on a simplified model with only two tubes in parallel or series (Figs. 3b-c). First, assuming two cylindrical tubes with radii r_1, r_2 in series, the flow is the same for the two tubes $q_1 = q_2 = q$ (Fig. 3b). The radius of each tube then changes as $dr_i/dt = \alpha q^m / r_i^n$ where $i = 1, 2$. As a result, we find that the conductivity of each tube changes as $dC_i/dt \propto q^m C_i^{(3-n)/4}$, where each tube's conductivity increases. Considering the pressure at the junction between tubes, we find that it moves toward the average value of pressure on both sides (Fig. 3(b₁)). Contrary to tubes in series, when the tubes are in parallel (Fig. 3c), the flow divides between the two tubes in proportion to their conductivity, i.e., $q_1/q_2 = C_1/C_2$. Since each tube's radius changes as $dr_i/dt = \alpha q_i^m / r_i^n$, the evolution of the fluid flow ratio becomes

$$\frac{d}{dt} \left(\frac{C_1}{C_2} \right) \propto \frac{C_1}{C_2^{n/4+1}} \left(\left(\frac{C_1}{C_2} \right)^{m-\frac{n+1}{4}} - 1 \right). \quad (3)$$

When $m = (n+1)/4$ in Eq. (3), the right-hand-side vanishes and as a result the flow ratio C_1/C_2 remains constant (Fig. 3c₁). However, when $m \neq (n+1)/4$,

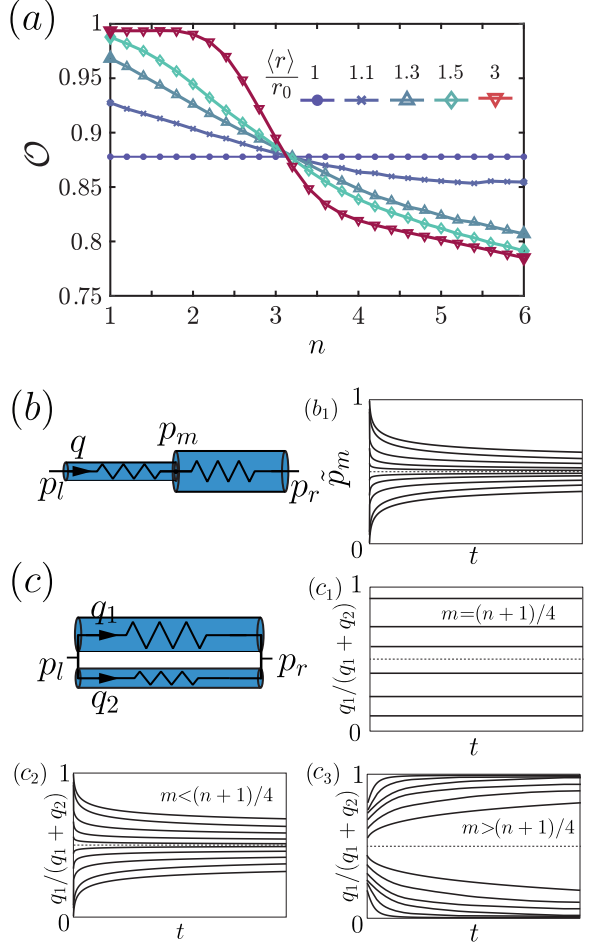


FIG. 3. (a) Order parameter \mathcal{O} calculated from simulation results presented in Fig. 2 for different powers of n with $m = 1$ plotted over time. (b,c) Tubes in series (b) or parallel (c) configuration. The tube radius dynamically change with the erosion law (Eq. (1)). When the tubes are in series, for any m, n , (b₁) the normalized pressure at the middle junction between the tubes $\tilde{p}_m = (p_m - p_l)/(p_r - p_l)$ approaches 1/2 which results in a homogenized pressure distribution. When the tubes are in parallel, for (c₁) $m = (n+1)/4$, the flow ratio between the pipes does not change over time; (c₂) $m < (n+1)/4$ the flow distributes between the tubes equally and $q_1/(q_1 + q_2) \rightarrow 1$ which results in the homogenization of the network; (c₃) $m > (n+1)/4$, the entire flow eventually passes through one of the tubes, and channeling occurs.

we find that $C_1/C_2 = 1$ is an equilibrium point. When $m < (n+1)/4$ this equilibrium solution is stable and the flow moves toward homogenization (Fig. 3c₂); however, when $m > (n+1)/4$ this equilibrium solution becomes unstable and the solution moves toward $C_1/C_2 \rightarrow 0$ or ∞ which means that the entire flow passes through one of the tubes (Fig. 3c₃). In summary, when the tubes are in series any erosion law makes flow become more uniform; however, when the tubes are in parallel depending on the powers m, n the flow in the tubes can move to-

ward becoming more uniform ($m < (n + 1)/4$), maintain the same ratio ($m = (n + 1)/4$), or move toward instability and channel development ($m > (n + 1)/4$). Since a complex network includes both series and parallel connections, it is plausible that the whole network structure will behave in a similar manner, with a transition in the networks behavior at $m = (n + 1)/4$. This observation is consistent with the numerical simulation results shown in Figs. 2 and 3a (for $m = 1$) as well as for additional values of m (Fig. 4).

Analysis of generalized model— So far we focused on erosion dynamics with $m = 1$ (Eq. (1)) since it directly corresponds to erosion laws of interest, i.e. an erosion rate with a linear dependence to fluid-flux, velocity, or shear-rate at the walls. Considering $m = 2$ in Eq. (1), our model aligns with the transport optimization problem in biological networks [41, 42, 44]. Previous works have suggested that in the context of biological transport networks, the network is optimized to minimize its dissipation energy with regards to some constraint (such as constant material or metabolic cost). Interestingly, the gradient descent method utilized to find the minimal energy configurations maps to Eq. (1) with $m = 2$, albeit with additional regularizing terms. While under the dynamics we study here erosion will occur indefinitely, in these biological network models a minimal energy configuration exists due to these additional constraints. Nonetheless, the minimal energy configurations manifest a phase transition reminiscent of the one we observe in our model. To test the role of the parameter m in our model, we simulated the general form of erosion dynamics (Eq. (1)). The simulation results for a randomly initialized network for different powers of m and n are shown in Fig. 4, where each box shows the final snapshot of the network eroded with the corresponding m and n . We further compare the network's simulation result with the prediction of our simplified model for the fate of the network for each pair of m, n . The simplified model's prediction is shown using the bounding box color (red for channelization and green for homogenization) in Fig. 4 (cf. Fig. S5 in supplementary material showing the heat map for the average change in the order parameter). Additionally, the dashed black line in Fig. 4 shows the simplified model's prediction for the boundary between network's transition to homogeneity or channelization (i.e., $m = (n + 1)/4$). Although the simplified model is based on the erosion dynamics of two edges in a parallel or series configuration, it still correctly predicts the fate of the network with the complex topology for different values of m and n , and captures the boundary separating channelization/homogenization.

In the case of clogging, the initial dynamics can similarly be captured using our model, however, due to the change in the connectivity of the network, our simplified model cannot extend to large time behaviors (supplementary material S5).

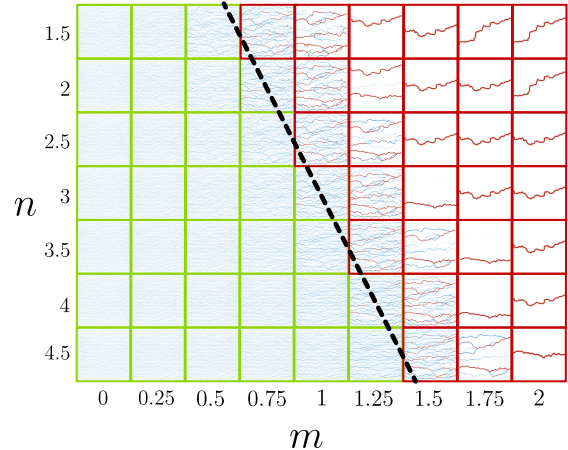


FIG. 4. Evolution of a randomly initialized network for various powers of m and n in Eq. (1). The network is randomly initialized with 50×50 randomly distributed pores. The bounding box color shows the prediction of the simplified model for the fate of the network: homogenization (blue) or channelization (red). The dashed black line shows the transition boundary between channelization instability and homogenization obtained using simplified model, i.e., $m = (n+1)/4$.

Conclusion— We analyzed the dynamics of porous networks during erosion. We showed that depending on the form of the erosion law (namely, its dependence on flux and tube radius) the network can either move towards homogenization or towards developing a channeling instability. We elucidated the physical origin of this phase transition and how it is achieved using a simplified model. Our results highlight the importance of local dynamics and feedback mechanisms in the network's path toward its asymptotic global behavior [41, 42, 44–46], and allow us to infer the local dynamics using large scale observations. As a result, our model can be used as a bulk behavior proxy for determining the local dynamics of erosion in a system [21]. Interestingly, our results indicates that an erosion model that is local and linearly dependent on shear rate cannot result in channelization (since $m = 1, n = 3$ and $m = (n + 1)/4$). However, we note that if the dependence on the shear rate is non-linear, it will qualitatively map to our model albeit with renormalized values of n and m : e.g., a power-law dependence on shear rate with exponent s would lead to $m = s, n = 3s$, implying channelization when $s > 1$. In the future, it would be exciting to test this and other predictions experimentally on model systems, relying on the technological advances in imaging flow profiles in porous materials, as well as extend the study to the geologically relevant case of chemical erosion [47, 48].

We thank the Kavli Foundation, MRSEC DMR-2011754, and DMR-1420570 for their support. We thank Yaniv Edery, Eleni Katifori, and Chris Rycroft for useful

discussions.

-
- * A.Z. and D.P. contributed equally.
 † arielamir@seas.harvard.edu
- [1] S. Marbach, K. Alim, N. Andrew, A. Pringle, and M. P. Brenner, Physical Review Letters **117**, 178103 (2016).
 - [2] K. Alim, G. Amselem, F. Peaudecerf, M. P. Brenner, and A. Pringle, Proceedings of the National Academy of Sciences **110**, 13306 (2013).
 - [3] A. Tero, S. Takagi, T. Saigusa, K. Ito, D. P. Bebbert, M. D. Fricker, K. Yumiki, R. Kobayashi, and T. Nakagaki, Science **327**, 439 (2010).
 - [4] L. L. Heaton, E. López, P. K. Maini, M. D. Fricker, and N. S. Jones, Proceedings of the Royal Society B: Biological Sciences **277**, 3265 (2010).
 - [5] W. H. Schlesinger, Science **284**, 2095 (1999).
 - [6] K. Winkler and A. Nur, Geophysical Research Letters **6**, 1 (1979).
 - [7] M. Batzle and Z. Wang, Geophysics **57**, 1396 (1992).
 - [8] M. Duduta, B. Ho, V. C. Wood, P. Limthongkul, V. E. Brunini, W. C. Carter, and Y.-M. Chiang, Advanced Energy Materials **1**, 511 (2011).
 - [9] H. Sun, J. Zhu, D. Baumann, L. Peng, Y. Xu, I. Shakir, Y. Huang, and X. Duan, Nature Reviews Materials **4**, 45 (2019).
 - [10] R. B. Smith and M. Z. Bazant, Journal of The Electrochemical Society **164**, E3291 (2017).
 - [11] T. R. Ferguson and M. Z. Bazant, Journal of The Electrochemical Society **159**, A1967 (2012).
 - [12] M. N. Rad, N. Shokri, and M. Sahimi, Physical Review E **88**, 032404 (2013).
 - [13] J. Herzig, D. Leclerc, and P. L. Goff, Industrial & Engineering Chemistry **62**, 8 (1970).
 - [14] C. Tien and A. C. Payatakes, AIChE Journal **25**, 737 (1979).
 - [15] D. P. Jaisi, N. B. Saleh, R. E. Blake, and M. Elimelech, Environmental Science & Technology **42**, 8317 (2008).
 - [16] M. Carrel, V. L. Morales, M. A. Beltran, N. Derlon, R. Kaufmann, E. Morgenroth, and M. Holzner, Water Research **134**, 280 (2018).
 - [17] J. D. Seymour, J. P. Gage, S. L. Codd, and R. Gerlach, Physical Review Letters **93**, 198103 (2004).
 - [18] L. W. Lake, R. Johns, B. Rossen, G. A. Pope, *et al.*, *Fundamentals of Enhanced Oil Recovery*, (2014).
 - [19] S. Parsa, E. Santanach-Carreras, L. Xiao, and D. A. Weitz, Physical Review Fluids **5**, 022001 (2020).
 - [20] N. Schorghofer, B. Jensen, A. Kudrolli, and D. H. Rothman, Journal of Fluid Mechanics **503**, 357 (2004).
 - [21] A. Mahadevan, A. Orpe, A. Kudrolli, and L. Mahadevan, Europhysics Letters **98**, 58003 (2012).
 - [22] L. T. Akanji and S. K. Matthai, Transport in Porous Media **81**, 241 (2010).
 - [23] I. Fatt *et al.*, Transactions of the AIME **207**, 144 (1956).
 - [24] M. J. Blunt, B. Bijeljic, H. Dong, O. Gharbi, S. Iglauder, P. Mostaghimi, A. Paluszny, and C. Pentland, Advances in Water resources **51**, 197 (2013).
 - [25] N. Stoop, N. Waisbord, V. Kantsler, V. Heinonen, J. S. Guasto, and J. Dunkel, Journal of Non-Newtonian Fluid Mechanics **268**, 66 (2019).
 - [26] S. L. Bryant, P. R. King, and D. W. Mellor, Transport in porous media **11**, 53 (1993).
 - [27] H. Dong and M. J. Blunt, Physical Review E **80**, 036307 (2009).
 - [28] M. J. Blunt and H. Scher, Physical Review E **52**, 6387 (1995).
 - [29] K. Alim, S. Parsa, D. A. Weitz, and M. P. Brenner, Physical Review Letters **119**, 144501 (2017).
 - [30] S. Parsa, A. Zareei, E. Santanach-Carreras, E. Morris, A. Amir, L. Xiao, and D. A. Weitz, submitted (2021).
 - [31] D. Fragedakis, E. Chaparian, and O. Tammisola, Journal of Fluid Mechanics **911**, A58 (2021).
 - [32] S. S. Datta, H. Chiang, T. Ramakrishnan, and D. A. Weitz, Physical Review Letters **111**, 064501 (2013).
 - [33] R. Jäger, M. Mendoza, and H. J. Herrmann, Physical Review E **95**, 013110 (2017).
 - [34] L. Ristroph, M. N. Moore, S. Childress, M. J. Shelley, and J. Zhang, Proceedings of the National Academy of Sciences **109**, 19606 (2012).
 - [35] W. Hacking, E. VanBavel, and J. Spaan, American Journal of Physiology-Heart and Circulatory Physiology **270**, H364 (1996).
 - [36] C. F. Wan and R. Fell, Journal of Geotechnical and Geoenvironmental Engineering **130**, 373 (2004).
 - [37] H. Steeb, S. Diebels, and I. Vardoulakis, “Modeling internal erosion in porous media,” in *Computer Applications In Geotechnical Engineering*, pp. 1–10.
 - [38] D. Marot, V. D. Le, J. Garnier, L. Thorel, and P. Audrain, European Journal of Environmental and Civil Engineering **16**, 1 (2012).
 - [39] L. Sibille, F. Lominé, P. Poullain, Y. Sail, and D. Marot, Hydrological Processes **29**, 2149 (2015).
 - [40] N. J. Derr, D. C. Fronk, C. A. Weber, A. Mahadevan, C. H. Rycroft, and L. Mahadevan, Physical Review Letters **125**, 158002 (2020).
 - [41] D. Hu and D. Cai, Physical Review Letters **111**, 138701 (2013).
 - [42] H. Ronellenfitsch and E. Katifori, Physical Review Letters **117**, 138301 (2016).
 - [43] B. Kramer and A. MacKinnon, Reports on Progress in Physics **56**, 1469 (1993).
 - [44] F. Corson, Physical Review Letters **104**, 048703 (2010).
 - [45] E. Katifori, G. J. Szöllösi, and M. O. Magnasco, Physical review letters **104**, 048704 (2010).
 - [46] S. A. Ocko and L. Mahadevan, Physical Review Letters **114**, 134501 (2015).
 - [47] Y. Edery, A. Guadagnini, H. Scher, and B. Berkowitz, Water Resources Research **50**, 1490 (2014).
 - [48] Y. Edery, G. M. Porta, A. Guadagnini, H. Scher, and B. Berkowitz, Transport in Porous Media **115**, 291 (2016).